Molecular Mechanism of Action of Microtubule-Stabilizing Anticancer Agents

Prota, Andrea E ; Bargsten, Katja ; Zurwerra, Didier ; Field, Jessica J ; Díaz, José Fernando ; Altmann, Karl-Heinz ; Steinmetz, Michel O

Abstract: Microtubule-stabilizing agents (MSAs) are efficacious chemotherapeutic drugs widely used for the treatment of cancer. Despite the importance of MSAs for medical applications and basic research, their molecular mechanisms of action on tubulin and microtubules remain elusive. Here we determined high-resolution crystal structures of aß-tubulin in complex with two unrelated MSAs, zampanolide and epothilone A. Both compounds were bound to the taxane-pocket of ß-tubulin and used their respective side chain to induce structuring of the M-loop into a short helix. Because the M-loop establishes lateral tubulin contacts in microtubules, these findings explain how taxane-site MSAs promote microtubule assembly and stability. They further offer fundamental structural insights into the control mechanisms of microtubule dynamics.

DOI: https://doi.org/10.1126/science.1230582

Molecular Mechanism of Action of Microtubule-Stabilizing Anticancer Agents

Andrea E. Prota[1], Katja Bargsten[1], Didier Zurwerra[2], Jessica J. Field[3], José Fernando Díaz[4], Karl-Heinz Altmann[2], and Michel O. Steinmetz[1*]

[1]Biomolecular Research, Paul Scherrer Institut, Villigen PSI, Switzerland.

[2]Department of Chemistry and Applied Biosciences, Institute of Pharmaceutical Sciences, Swiss Federal Institute of Technology (ETH) Zürich, Zürich, Switzerland.

[3]Centre for Biodiscovery, Victoria University of Wellington, Wellington, New Zealand.

[4]Chemical and Physical Biology, Centro de Investigaciones Biológicas, Consejo Superior de Investigaciones Científicas CIB-CSIC, Madrid, Spain.

*To whom correspondence should be addressed. E-mail: michel.steinmetz@psi.ch

Abstract

Microtubule-stabilizing agents (MSAs) are efficacious chemotherapeutic drugs widely used for the treatment of cancer. Despite the importance of MSAs for medical applications and basic research, their molecular mechanisms of action on tubulin and microtubules remain elusive. Here we determined high-resolution crystal structures of αβ-tubulin in complex with two unrelated MSAs, zampanolide and epothilone A. Both compounds were bound to the taxane-pocket of β-tubulin and used their respective side chain to induce structuring of the M-loop into a short helix. Because the M-loop establishes lateral tubulin contacts in microtubules, these findings explain how taxane-site MSAs promote microtubule assembly and stability. They further offer fundamental structural insights into the control mechanisms of microtubule dynamics.

One sentence summary:

Microtubule-stabilizing agents use a common mechanism to stabilize a major loop in tubulin that controls microtubule assembly and stability.

The binding of MSAs like Taxol to microtubules is generally thought to shift the assembly equilibrium of tubulin towards the polymeric state and to block cell entry into mitosis by suppressing microtubule dynamics (*1, 2*). However, MSAs are also known to induce microtubule polymerization under conditions where tubulin does not assemble spontaneously, suggesting a role in tubulin activation (*3, 4*). To provide insights into the interactions of MSAs with tubulin and microtubules at the molecular level, we crystallized the complex between αβ-tubulin, the stathmin-like protein RB3 and tubulin tyrosine ligase (TTL) in the presence of either zampanolide (Zampa) or epothilone A (EpoA) (Fig. 1A), and determined the structures of the corresponding protein-ligand complexes (T_2R-TTL-Zampa and (T_2R-TTL-EpoA) by X-ray crystallography (Fig. S1A; Table S1) (*5*). The two tubulin heterodimers in the T_2R-TTL-MSA complexes were aligned in a head-to-tail fashion and assumed a curved conformation. Their overall structures superimposed well with the ones obtained in the absence of a MSA or of tubulin in complex with RB3 alone (*6*) (rmsd ranging from 0.1-0.6 Å over >650 Cα-atoms), suggesting that binding of MSAs and TTL does not induce significant structural changes in the T_2R complex. Both Zampa and EpoA were deeply buried in a pocket formed by predominantly hydrophobic residues of helix H7, β-strand S7, and the loops H6-H7, S7-H9 (designated the M-loop (*7*)) and S9-S10 of β-tubulin; this pocket is commonly known as the 'taxane-pocket' (*8, 9*) (Fig. 1, B-D).

In the T_2R-TTL-Zampa complex, the C9 atom of Zampa was covalently bound to the NE2 atom of His229 of β-tubulin (Fig. S1B), which is consistent with mass spectrometry data (*10*). In addition, two hydrogen bonds were formed between the OH20 group and the O1' atom of Zampa, and the main chain carbonyl oxygen and the NH group of Thr276, respectively. In the T_2R-TTL-EpoA complex, the O1, OH3, OH7 and N20 groups of EpoA were hydrogen bonded to atoms of residues Thr276 (main chain NH), Gln281 (side chain amide nitrogen), Asp226 (side chain oxygen) and Thr276 (side chain hydroxyl group) of β-tubulin, respectively. The binding

mode of EpoA in the tubulin-EpoA structure is fundamentally different from the one proposed based on electron crystallography data of zinc-stabilized tubulin sheets (Fig. S2A); however, the orientation of the ligand in the taxane-pocket was ambiguous in the electron crystallography structure because the density of the ligand in experimental omit maps was discontinuous and limited in quality (*9, 11*). In contrast, the density of EpoA in our tubulin-EpoA X-ray crystal structure is very well defined and allowed the orientation of the ligand as well as its conformation to be defined unambiguously (Fig. S1C).

A comparison of the tubulin-Zampa taxane-pocket with the one of tubulin-EpoA showed that its conformation is very similar in both complex structures (rmsd of 0.4 Å over 55 Cα-atoms), and revealed that the side chains of Zampa and EpoA superimposed well (Fig. S2B). In contrast, completely different sets of interactions were established by the two MSAs to anchor their macrolide core structures in the taxane-pocket, with the planes of the macrocycles oriented at a ~90° angle.

A hallmark of both the tubulin-Zampa and tubulin-EpoA complex structures was the presence of a short helix formed by residues Arg278-Tyr283 in the M-loop of β-tubulin (Fig. 2A). This segment was largely disordered in the absence of a MSA (Fig. 2B). In contrast, the other elements of the taxane-pocket superimposed well between the ligand-bound and -unbound states, suggesting that the binding of a MSA is not required to structure these parts of the pocket (rmsd of 0.2 Å over 77 Cα-atoms). The helical conformation of the M-loop induced upon ligand binding can be explained by the various hydrophobic and polar contacts established between the side chains of Zampa and EpoA, respectively, and residues of the M-loop (Fig. 1, C and D). The helix was further stabilized by a characteristic intramolecular hydrogen bonding network formed by residues of the M-loop and helix H9 of β-tubulin (Fig. 2C).

The ‘curved’ structure of tubulin in the tubulin-RB3 complex corresponds to the conformation of unassembled, free tubulin (*12, 13*). In contrast, a ‘straight’ conformation of

tubulin is found in microtubules (*8, 14*). To assess possible structural differences between the taxane-pocket in unassembled tubulin and microtubules, we compared models of β-tubulin in the curved (T_2R-TTL-Zampa) and straight (*14*) conformational states. Superimposition of these structures showed that the overall architecture of the taxane-pocket is only slightly affected by the curved-to-straight structural rearrangements (rmsd of 1.1 Å over 73 Cα-atoms; Fig. 3A). This observation is in agreement with biochemical studies suggesting that some MSAs can bind to unassembled and/or oligomeric forms of tubulin (*10, 15*). The stronger binding of MSAs to microtubules can be explained by the disordered nature of the M-loop in unassembled tubulin in comparison to its structured state in microtubules (*7, 16*).

The M-loop of both α- and β-tubulin is a crucial element for lateral tubulin contacts between protofilaments in microtubules in the absence of ligands (*7, 16*). To provide structural insights into lateral tubulin contacts we modeled the helical conformation of the M-loop in the context of the microtubule lattice. For this purpose, we used the straight tubulin structure (*14*) and cryo-electron microscopy reconstructions of microtubules at ~8 Å resolution (*7, 16*). In contrast to the non-native M-loop conformation in zinc-stabilized tubulin sheets (*14*), the MSA-stabilized helical M-loop conformation of β-tubulin explains well the corresponding density of electron microscopy reconstructions of microtubules (Fig. 3B). In our model, Tyr283 of the M-loop is inserted across protofilaments into a pocket shaped by the S2'-S2'' β-hairpin and the H2-S3 loop (residues Ala56, Thr57, Val62, Gln85, Arg88, Pro89 and Asp90) of a neighboring β-tubulin subunit (Fig. 3C), secondary structure elements that were not significantly affected by the curved-to-straight tubulin conformational transition (Fig. 3A; rmsd of 0.7 Å over 91 Cα-atoms). In addition, the M-loop residues Ser280, Gln282, Arg284 and Ala285 were favorably positioned to form additional contacts to the neighboring β-tubulin. The M-loop of α-tubulin in our tubulin-MSA complexes was also stabilized in a similar helical conformation, in this case due to a crystal contact (Fig. S3). In combination with molecular dynamics simulations (*17*),

these data collectively suggest that the disordered M-loops of both α- and β-tubulin exhibit an intrinsic propensity to form a helix that establishes lateral tubulin contacts in microtubules.

Our study provides fundamental structural information on the molecular mechanism of action of MSAs (Fig. 3D). Apart from additional global effects (*17-19*), a common feature of tubulin activation by MSAs is the formation of a short helix in the M-loop of β-tubulin upon MSA binding. As M-loop structuring is a crucial prerequisite for lateral tubulin interactions, this effect explains how MSAs promote microtubule assembly and stabilization. Our data further suggest that the intramolecular interaction network that stabilizes the M-loop helix of both α- and β-tubulin also forms in microtubules in the absence of a ligand. We propose that the helical structuring of the M-loop facilitates the curved-to-straight conformational change that occurs upon incorporation of tubulin into microtubules. In this context, the binding of a MSA leads to tubulin pre-organization according to the gross structural requirements of the assembly process, thus reducing the entropy loss associated with microtubule formation. Our model implies in turn that dissolution of the helical structure of the M-loops is an early molecular event in the process of microtubule disassembly.

The high-resolution structural information obtained for the tubulin-MSA complexes reported here opens the possibility for structure-guided drug engineering. While the structure-activity relationship of epothilones has been explored extensively (*20*) and one epothilone derivative, ixabepilone, has been approved by the FDA for breast cancer treatment (*21*), little structure-activity work has been reported on Zampa (*22*). Zampa exhibits favorable properties that could make it an attractive lead compound (*10*). It is a very potent MSA that exerts its action through covalent binding to tubulin, which might provide superior activity in the case of P-glycoprotein-mediated multidrug resistance.

References and Notes

1. C. Dumontet, M. A. Jordan, *Nat. Rev. Drug Discov.* **9**, 790 (2010).
2. P. B. Schiff, J. Fant, S. B. Horwitz, *Nature* **277**, 665 (1979).
3. J. F. Diaz, J. M. Andreu, *Biochemistry* **32**, 2747 (1993).
4. J. F. Diaz, M. Menendez, J. M. Andreu, *Biochemistry* **32**, 10067 (1993).
5. Materials and methods are available as supplementary materials on *Science* Online.
6. R. B. Ravelli *et al.*, *Nature* **428**, 198 (2004).
7. E. Nogales, M. Whittaker, R. A. Milligan, K. H. Downing, *Cell* **96**, 79 (1999).
8. E. Nogales, S. G. Wolf, K. H. Downing, *Nature* **391**, 199 (1998).
9. J. H. Nettles *et al.*, *Science* **305**, 866 (2004).
10. J. J. Field *et al.*, *Chem. Biol.* **19**, 686 (2012).
11. J. H. Nettles, K. H. Downing, *Top. Curr. Chem.* **286**, 209 (2009).
12. P. Ayaz, X. Ye, P. Huddleston, C. A. Brautigam, L. M. Rice, *Science* **337**, 857 (2012).
13. L. Pecqueur *et al.*, *Proc. Natl. Acad. Sci. U. S. A* **109**, 12011 (2012).
14. J. Lowe, H. Li, K. H. Downing, E. Nogales, *J. Mol. Biol.* **313**, 1045 (2001).
15. M. Reese *et al.*, *Angew. Chem. Int. Ed Engl.* **46**, 1864 (2007).
16. F. J. Fourniol *et al.*, *J. Cell Biol.* **191**, 463 (2010).
17. A. Mitra, D. Sept, *Biophys. J.* **95**, 3252 (2008).
18. C. Elie-Caille *et al.*, *Curr. Biol.* **17**, 1765 (2007).
19. H. Xiao *et al.*, *Proc. Natl. Acad. Sci. U. S. A* **103**, 10166 (2006).
20. K.-H. Altmann, B. Pfeiffer, S. Arseniyadis, B. A. Pratt, K. C. Nicolaou, *ChemMedChem.* **2**, 396 (2007).
21. R. J. Lechleider *et al.*, *Clin. Cancer Res.* **14**, 4378 (2008).
22. D. Zurwerra *et al.*, *Chem. Eur. J.* (2012).

Acknowledgements

We are indebted to R. Kammerer, F. Winkler, Y. Barral for critical reading of the manuscript, and to V. de Lucas de Segovia for providing calf brains for tubulin purification. We thank V. Olieric for excellent technical assistance with the collection of X-ray data at beamline X06SA and X06DA of the Swiss Light Source (Paul Scherrer Institut, Villigen, Switzerland). JJF received a short-term fellowship from EMBO and a Professional Development Grant from the Genesis Oncology Trust. This work was supported by grants from the Ministerio de Economía y Competitividad (BIO2010-16351) and the Comunidad Autónoma de Madrid (S2010/BMD-2457) (to JFD), by a PhD fellowship from the Roche Research Foundation (to DZ), and by grants from the Swiss National Science Foundation (310030B_138659) and the Swiss SystemsX.ch initiative (BIP-2011/122) (to MOS). Coordinates have been deposited at the Protein Data Bank (PDB) under accession numbers 4I4T (T_2R-TTL-Zampa), 4I50 (T_2R-TTL-EpoA) and 4I55 (T_2R-TTL).

Supplementary Materials

www.sciencemag.org

Materials and Methods

Figs. S1 to S3

Table S1

References 23-30

Figure Legends

Fig. 1. Tubulin-Zampa and tubulin-EpoA complex structures. (**A**) Chemical structure of (-)-Zampa and EpoA. (**B**) Overall view of the complex formed between tubulin (gray surface; M-loop in yellow) and Zampa (green spheres). The dashed box depicts the area shown in more details in panel (**C**). (**C**) and (**D**) Close up views of the interaction network observed between Zampa (green sticks; panel **C**) or EpoA (light green sticks; panel **D**) and β-tubulin (gray cartoon). Interacting residues of β-tubulin are shown in stick representation. Oxygen and nitrogen atoms are colored in red and blue, respectively, carbon atoms in green (Zampa and EpoA) or gray and yellow (β-tubulin). Hydrogen bonds are depicted as black dashed lines. The covalent bond between the C9 atom of Zampa and the NE2 atom of His229 is indicated by an orange stick.

Fig. 2. Conformation of the M-loop of β-tubulin. (**A**) and (**B**) 2mFo-DFc (grey mesh, contoured at 1.0σ) and mFo-DFc (green and red mesh, +/- 3.0σ) electron density maps of the region surrounding the M-loop of β-tubulin in the T_2R-TTL-Zampa (**A**) and T_2R-TTL (**B**) complexes. (**C**) Close up view of the Zampa-induced intramolecular interaction network that contributes to the stabilization of the M-loop helix.

Fig. 3. Lateral tubulin interactions in microtubules. (**A**) Superimposition of the taxane-pocket (right) and M-loop-contacting elements across protofilaments (left) in curved (T_2R-TTL-Zampa; gray) and straight (PDP ID 1JFF; light blue) β-tubulin. (**B**) 8.2 Å cryo-electron microscopy map of a microtubule viewed from its luminal side (gray surface; EMDB-map 1788). Two chimeric molecules composed of straight β-tubulin (cartoon representation) and elements shaping the taxane-pocket in the curved tubulin-Zampa complex (**A**) are fitted in the map. (**C**) Close up view of the lateral β-tubulin contact model shown in panel (**B**). (**D**) Proposed molecular mechanism of

action of MSAs on tubulin and microtubules. (1) Binding of a MSA (rhomboid) to the taxane-site structures the disordered M-loop of β-tubulin (dashed line) into a helix (cylinder). (2) The MSA-stabilized M-loop promotes tubulin polymerization. (3) The M-loop helices of α- and β-tubulin are also formed in the context of the microtubule in the absence of a ligand. (4) All taxane-site MSAs bind to tubulin in the microtubule to stabilize lateral contacts. For more details, see text.

Figure 1

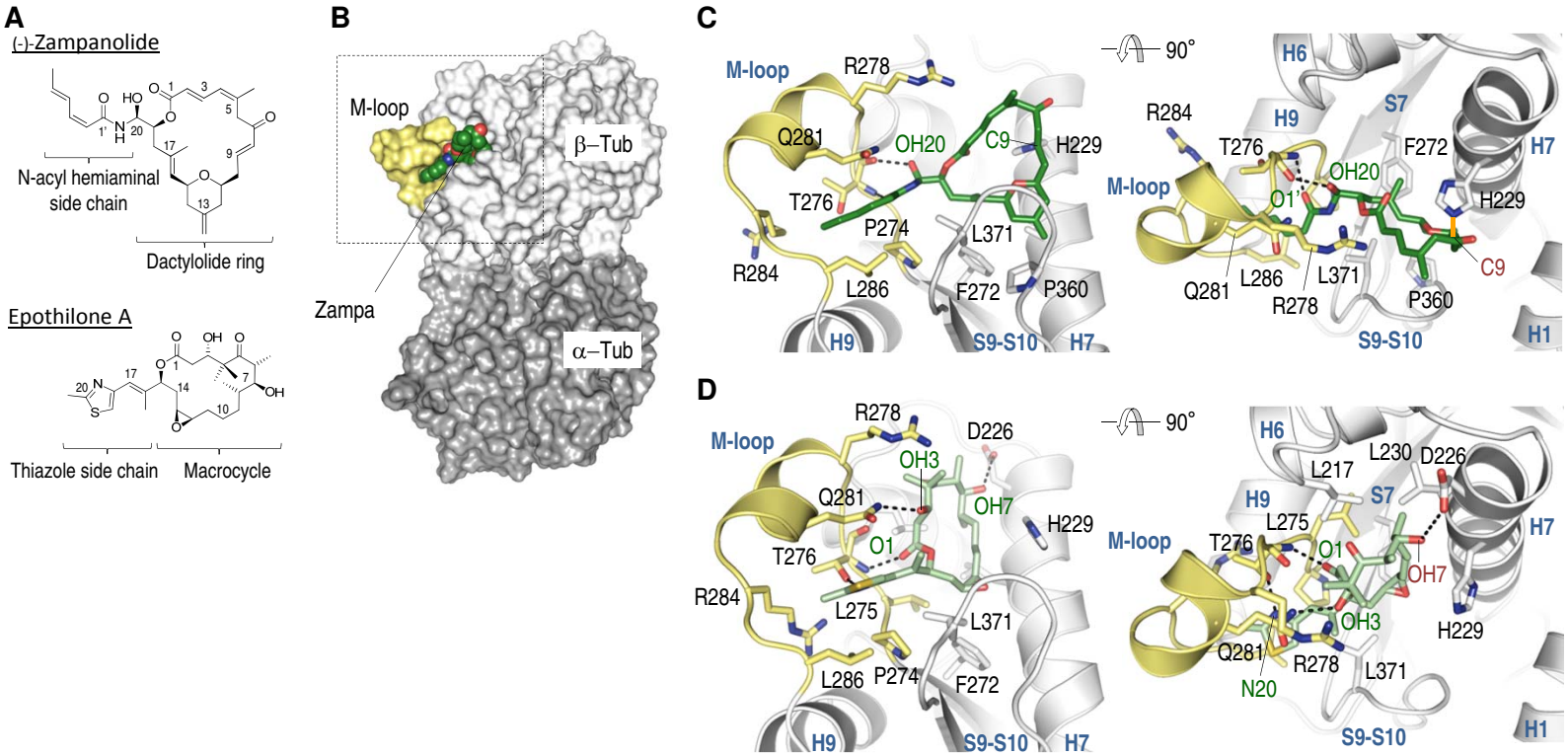
A
(-)-Zampanolide
N-acyl hemiaminal side chain
Dactylolide ring
Epothilone A
Thiazole side chain
Macrocycle
B
M-loop
β–Tub
α–Tub
Zampa
C
M-loop
R278
Q281
OH20
C9
H229
T276
P274
L371
R284
L286
F272
P360
H9
S9-S10
H7
90°
H6
S7
H9
R284
T276
F272
H7
OH20
M-loop
O1'
H229
C9
Q281
L286
L371
R278
P360
S9-S10
H1
D
R278
D226
M-loop
OH3
Q281
OH7
H229
T276
O1
R284
L275
L371
L286
P274
F272
H9
S9-S10
H7
90°
H6
L230
D226
L217
H9
S7
L275
H7
M-loop
T276
O1
OH7
OH3
H229
Q281
R278
L371
N20
S9-S10
H1

Figure 2

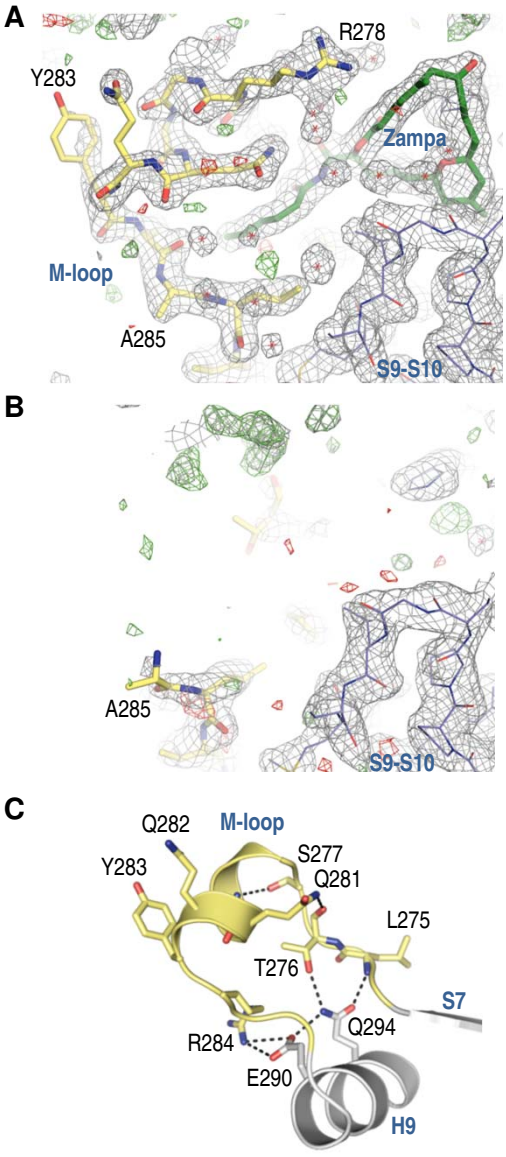
A
R278
Y283
Zampa
M-loop
A285
S9-S10
B
A285
S9-S10
C
Q282
M-loop
S277
Y283
Q281
L275
T276
S7
Q294
R284
E290
H9

Figure 3

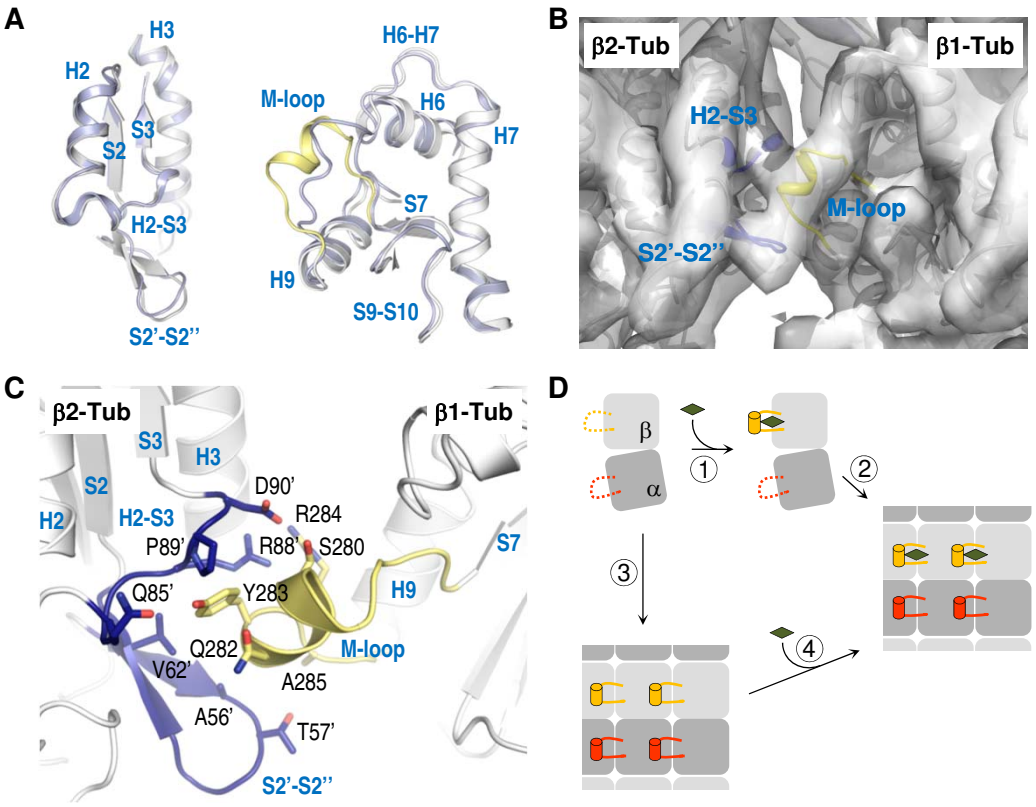
A
H3
H2
S3
S2
H2-S3
S2'-S2''
H6-H7
M-loop
H6
H7
S7
H9
S9-S10
B
β2-Tub
β1-Tub
H2-S3
M-loop
S2'-S2''
C
β2-Tub
β1-Tub
S3
H3
S2
H2
H2-S3
D90'
R284
P89'
R88'
S280
S7
Q85'
Y283
H9
Q282
M-loop
V62'
A285
A56'
T57'
S2'-S2''
D
β
α
①
②
③
④

Supplementary Materials for

Molecular Mechanism of Action of Microtubule-Stabilizing Anticancer Agents

Andrea E. Prota, Katja Bargsten, Didier Zurwerra, Jessica J. Field, José Fernando Díaz, Karl-Heinz Altmann, and Michel O. Steinmetz*

correspondence to: michel.steinmetz@psi.ch

This PDF file includes:

Materials and Methods

Protein and MSA preparation

The gene encoding the chicken TTL orthologue was initially cloned from chicken whole brain cDNA (BioChain), and then transferred into the negative selection vector NSKn1 (*23*) with a C-terminal hexahistidine tag. Recombinant TTL was overexpressed in the *E. coli* strain BL21 (DE3). Cells were grown at 37°C in LB medium supplemented with 50 mg/l kanamycin to reach an OD_{600} of 1.2. After induction with 1 mM IPTG the cultures were shaken at 20°C for 20 h. Cells were harvested by centrifugation, resuspended in lysis buffer (50 mM Tris pH 7.5, 1 M NaCl, 10% glycerol, 2.5 mM $MgCl_2$) supplemented with 10 mM β-ME, protease inhibitors (1 tablet complete (Roche) / 50 ml buffer) and DNAse, and disrupted using an Emulsiflex homogenizer. The lysate was clarified by centrifugation at 100,000 g for 45 min and loaded onto a 5 ml HisTrap affinity column (GE Healthcare), washed with 20 mM imidazole and eluted with a gradient from 20 to 250 mM imidazole in 20 column volumes. The fractions containing TTL protein were pooled, concentrated to 5 ml using a Centriprep (Amicon; Mw cutoff 30,000) and loaded onto a Superdex 200 16/60 column for the final purification step in 20 mM Bis Tris Propane, pH 6.5 supplemented with 200 mM NaCl, 2.5 mM $MgCl_2$, 5 mM β-mercaptoethanol and 1% glycerol. The protein containing fractions were collected, concentrated to ~20 mg/ml and frozen in aliquots in liquid nitrogen for storage.

Bovine brain tubulin was prepared according to well established protocols (*24*). The stathmin-like domain clone of RB3 was a kind gift by A. Sobel. The protein was prepared according to (*6*). The total synthesis of (-)-zampanolide (Zampa) has been reported (*22*). Epothilone A (EpoA) was a kind gift of Novartis Pharma.

Crystallization, data collection and structure solution

The Zampa adduct (TZ) was prepared by a 1 hour incubation of tubulin (3 mg/ml) at 4°C in the presence of a slight molar excess of the compound. The T_2R-TTL-Zampa complex was formed by mixing the individual components at a ratio of 2:1.3:1.2 (TZ:RB3:TTL) supplemented with 1 mM AMPPCP, 5 mM tyrosinol and 10 mM DTT, and concentrated to 20 mg/ml prior to crystallization. The T_2R-TTL-EpoA complex was prepared by mixing 20 mg/ml T_2R-TTL with 0.5 mM EpoA, 1 mM AMPPCP, 5 mM tyrosine and 10 mM DTT. The T_2R-TTL complex without MSA was prepared by mixing 20 mg/ml T_2R-TTL with 1 mM AMPPCP, 5 mM tyrosinol and 10 mM DTT.

T_2R-TTL and T_2R-TTL-MSA complexes were crystallized by the sitting-drop vapor-diffusion method at 20°C. Crystals grew over night in precipitant solution consisting of 3% PEG 4K, 4-6% glycerol, 30 mM $MgCl_2$, 30 mM $CaCl_2$, 100 mM MES/Imidazole pH 6.7 and reached their maximum dimensions within one week. They belonged to space group $P2_12_12_1$, with one T_2R-TTL-MSA complex in the asymmetric unit. Native data were collected at 100K at beamlines X06SA and X06DA of the Swiss Light Source (SLS, Villigen PSI). Data were processed and merged with XDS (*25*). The structure was determined by molecular replacement with PHASER (*26*) using the individual components of the complex as search models (PDB IDs 3RYC and 3TIN). The initial molecular replacement model was first fitted by rigid body refinement followed by simulated annealing and restrained refinement in Phenix (*27*) with riding hydrogens. The resulting model was further improved through iterative model rebuilding in Coot (*28*) and

refinement in Phenix. NCS restraints were applied in initial refinement stages and then omitted in the final cycles of refinement to account for structural variations between the ncs-related copies of α- and β-tubulin. TLS-refinement was included in the final cycles of refinement. The quality of the structure was assessed with MolProbity (*29*). Data collection and refinement statistics are given in Table S1.

Structural analysis and figure preparation

Figures were prepared using PyMOL (The PyMOL Molecular Graphics System, Version 1.4.1. Schrödinger, LLC). Chains in the T_2R-TTL complex were defined as follows: chain A, α1-tubulin; chain B, β1-tubulin; chain C, α2-tubulin; chain D, β2-tubulin; chain E, RB3; chain F, TTL. See also Fig. S1A.

Chains C and D were used throughout for the structural analyses and figure preparation. The M-loop and MSA in chain B is less well defined. We thus decided not to model these elements in chain B. In contrast, the electron density of the M-loop and MSA in chain D allowed for a full modeling of this site in the β2-tubulin molecule (Fig. 2A).

Structural comparison and modeling of the 'curved' and 'straight' (PDB ID 1JFF) tubulin structures (Fig. 3) was performed by superimposing the N-terminal nucleotide-binding and C-terminal domains of β-tubulin (*6*).

The tubulin-TTL interaction is described in details in (*31*).

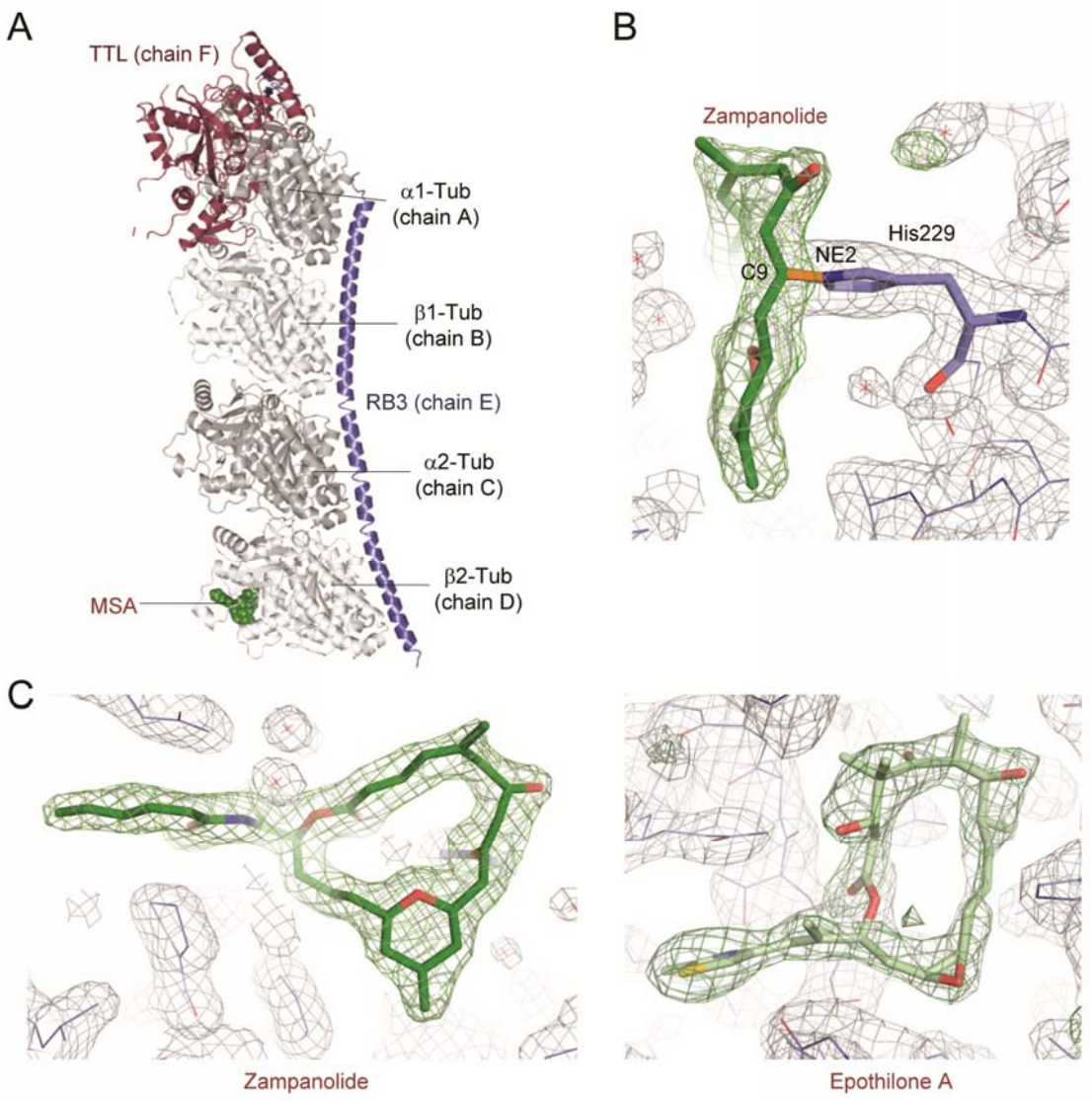

Fig. S1. Overall structure of the T_2R-TTL-MSA complex and covalent binding of Zampa to His229 of β-tubulin.

(**A**) Overall structure of the 2:1:1:1 αβ–tubulin-RB3-TTL-MSA complex. Tubulin (gray), TTL (raspberry) and RB3 (blue) are shown in cartoon representations; the MSA (Zampa) is depicted in green spheres representation. (**B**) Simulated annealing omit maps of the Zampa binding site showing the covalent link to His229 of β-tubulin. The SigmaA-weighted 2mFo-DFc (grey mesh) and mFo-DFc (green mesh) electron density maps are contoured at 1.0σ and +/- 3.0σ, respectively. The Zampa molecule (green) and His229 (cyan) are in stick representation. (**C**) Simulated annealing omit maps of the Zampa (left panel) and EpoA (right panel) binding sites. The SigmaA-weighted 2mFo-DFc (grey mesh) and mFo-DFc (green mesh) electron density maps are contoured at 1.0σ and +/- 3.0σ, respectively. The Zampa and EpoA molecules are shown in dark and light green stick representation, respectively.

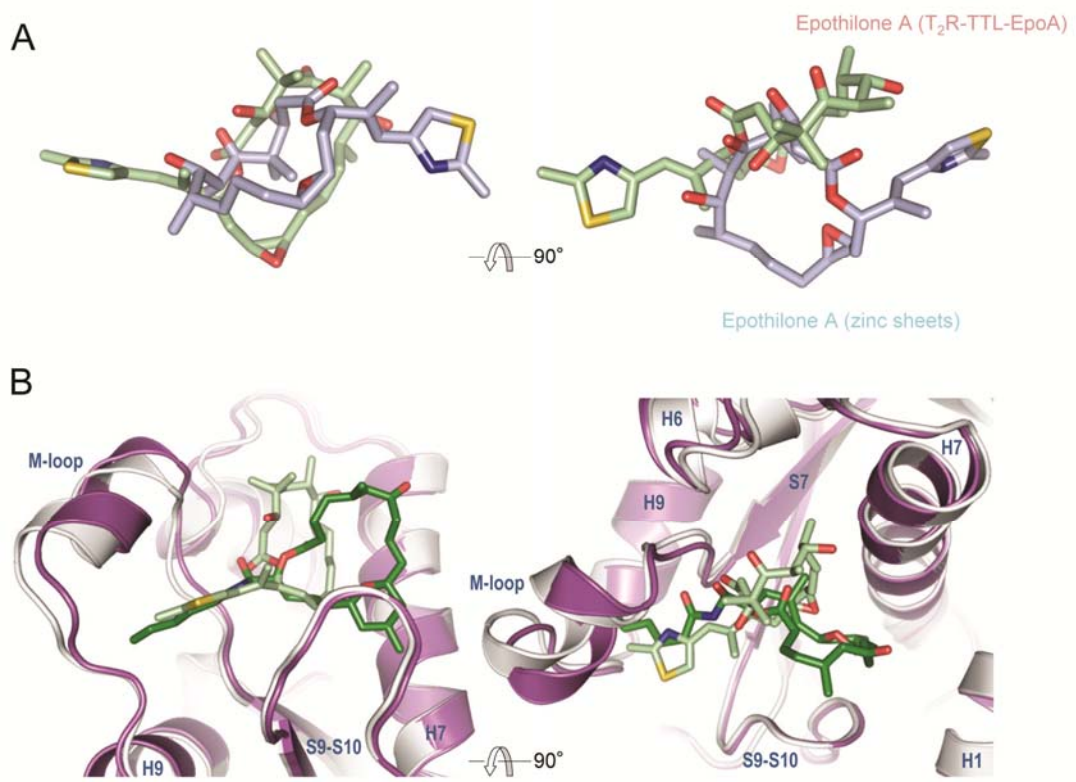

Fig. S2. Comparison of EpoA and Zampa in different complex structures with tubulin.

(**A**) The structure of EpoA bound in the taxane-pocket of 'straight' tubulin (obtained from zinc sheets (cyan; PDB ID 1TVK)) is superimposed onto the one observed in 'curved' tubulin (light green; T2R-TTL-EpoA). (**B**) Close up views of the superimposition of the tubulin-Zampa (gray) and tubulin-EpoA (magenta) complex structures. The Zampa and EpoA molecules are shown in dark and light green stick representation, respectively.

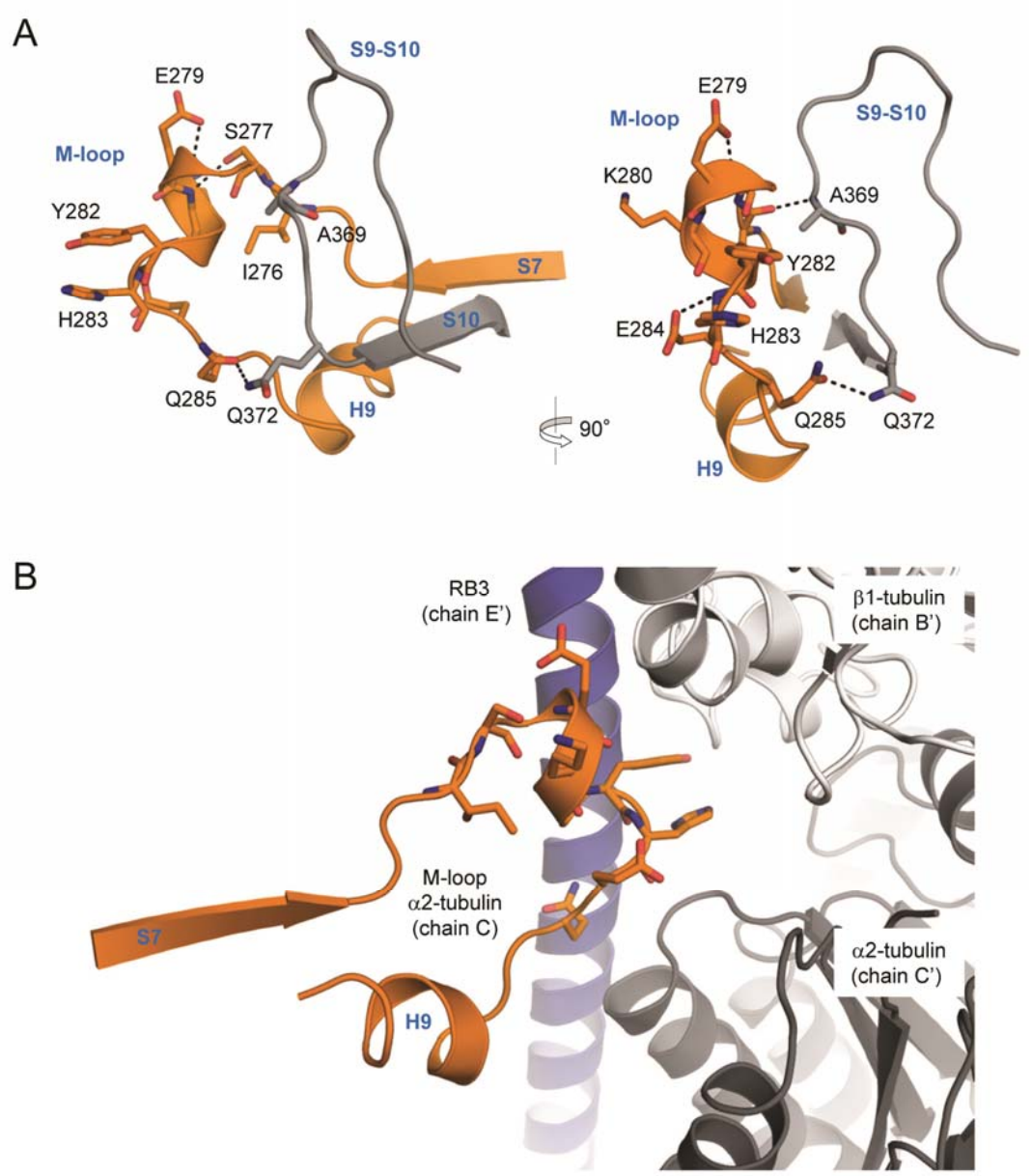

Fig. S3. Conformation of the M-loop of α-tubulin in T_2R-TTL-MSA.

(**A**) The M-loop of α-tubulin is stabilized in a helical conformation by a crystal contact shown in (**B**) and by an intermolecular hydrogen-bonding network (black dashed lines). Secondary structure elements are shown in cartoon representation; residue side chains are shown in stick representation. β-strand S7, the M-loop and helix H9 are colored in orange; the S9-S10 loop and β-strand S10 in gray (only depicted in panel (**A**)). In panel (**B**), RB3 (blue), α- and β-tubulin (dark and light gray, respectively) of a neighboring T_2R-TTL-MSA complex in the crystal are depicted.

Table S1. Data collection and refinement statistics.
[a]Highest shell statistics are in parentheses. [b]As defined by Karplus & Diederichs (*30*). [c]As defined by MolProbity (*29*).

Data collection[a]	T_2R-TTL-Zampa	T_2R-TTL-EpoA	T_2R-TTL
Space group	$P2_12_12_1$	$P2_12_12_1$	$P2_12_12_1$
Cell dimensions			
a, b, c (Å)	104.8, 158.6, 179.2	103.6, 155.1, 180.4	104.2, 156.5, 181.5
Resolution (Å)	79.4 – 1.80 (1.85 – 1.80)	77.6 – 2.3 (2.36 -2.30)	71.8 - 2.2 (2.26 – 2.20)
R_{meas} (%)	10.7 (256.5)	13.6 (248.5)	9.7 (130.9)
R_{pim} (%)	3.1 (74.6)	4.0 (71.5)	3.3 (98.0)
CC_{half}[b]	99.9 (53.7)	99.9 (47.7)	99.9 (64.7)
$\langle I \rangle / \langle \sigma I \rangle$	13.4 (1.0)	13.8 (1.2)	16.2 (2.2)
Completeness (%)	99.8 (99.0)	100 (100)	99.2 (93.9)
Redundancy	13.5 (13.1)	13.6 (13.8)	13.2 (11.9)
Refinement			
Resolution (Å)	79.4 – 1.80	77.6 – 2.3	71.8 – 2.2
No. unique reflections	274515 (13945 in test set)	129379 (6505 in test set)	149390 (7514 in test set)
R_{work}/R_{free} (%)	17.2 / 20.5	19.0 / 24.6	16.8 / 20.8
Average B-factors (Å^2)			
complex	44.1	66.0	55.7
solvent	48.1	51.2	50.4
MSA (chain D)	40.0	64.7	-
R.m.s. deviation from ideality			
Bond length (Å)	0.008	0.005	0.008
Bond angles (°)	1.100	0.943	1.111
Ramachandran statistics[c]			
Favored regions (%)	98.3	97.4	97.8
Allowed regions (%)	1.6	2.5	2.1
Outliers (%)	0.1	0.1	0.1

References and Notes

1. C. Dumontet, M. A. Jordan, Microtubule-binding agents: a dynamic field of cancer therapeutics. *Nat. Rev. Drug Discov.* **9**, 790 (2010).

2. P. B. Schiff, J. Fant, S. B. Horwitz, Promotion of microtubule assembly in vitro by taxol. *Nature* **277**, 665 (1979).

3. J. F. Diaz, J. M. Andreu, Assembly of purified GDP-tubulin into microtubules induced by taxol and taxotere: reversibility, ligand stoichiometry, and competition. *Biochemistry* **32**, 2747 (1993).

4. J. F. Diaz, M. Menendez, J. M. Andreu, Thermodynamics of ligand-induced assembly of tubulin. *Biochemistry* **32**, 10067 (1993).

5. Materials and methods are available as supplementary materials on *Science* Online.

6. R. B. Ravelli *et al.*, Insight into tubulin regulation from a complex with colchicine and a stathmin-like domain. *Nature* **428**, 198 (2004).

7. E. Nogales, M. Whittaker, R. A. Milligan, K. H. Downing, High-resolution model of the microtubule. *Cell* **96**, 79 (1999).

8. E. Nogales, S. G. Wolf, K. H. Downing, Structure of the alpha beta tubulin dimer by electron crystallography. *Nature* **391**, 199 (1998).

9. J. H. Nettles *et al.*, The binding mode of epothilone A on alpha,beta-tubulin by electron crystallography. *Science* **305**, 866 (2004).

10. J. J. Field *et al.*, Zampanolide, a Potent New Microtubule-Stabilizing Agent, Covalently Reacts with the Taxane Luminal Site in Tubulin alpha,beta-Heterodimers and Microtubules. *Chem. Biol.* **19**, 686 (2012).

11. J. H. Nettles, K. H. Downing, The tubulin binding mode of microtubule stabilizing agents studied by electron crystallography. *Top. Curr. Chem.* **286**, 209 (2009).

12. P. Ayaz, X. Ye, P. Huddleston, C. A. Brautigam, L. M. Rice, A TOG:alphabeta-tubulin Complex Structure Reveals Conformation-Based Mechanisms for a Microtubule Polymerase. *Science* **337**, 857 (2012).

13. L. Pecqueur *et al.*, A designed ankyrin repeat protein selected to bind to tubulin caps the microtubule plus end. *Proc. Natl. Acad. Sci. U. S. A* **109**, 12011 (2012).

14. J. Lowe, H. Li, K. H. Downing, E. Nogales, Refined structure of alpha beta-tubulin at 3.5 A resolution. *J. Mol. Biol.* **313**, 1045 (2001).

15. M. Reese *et al.*, Structural basis of the activity of the microtubule-stabilizing agent epothilone a studied by NMR spectroscopy in solution. *Angew. Chem. Int. Ed Engl.* **46**, 1864 (2007).

16. F. J. Fourniol *et al.*, Template-free 13-protofilament microtubule-MAP assembly visualized at 8 A resolution. *J. Cell Biol.* **191**, 463 (2010).

17. A. Mitra, D. Sept, Taxol allosterically alters the dynamics of the tubulin dimer and increases the flexibility of microtubules. *Biophys. J.* **95**, 3252 (2008).

18. C. Elie-Caille *et al.*, Straight GDP-tubulin protofilaments form in the presence of taxol. *Curr. Biol.* **17**, 1765 (2007).

19. H. Xiao *et al.*, Insights into the mechanism of microtubule stabilization by Taxol. *Proc. Natl. Acad. Sci. U. S. A* **103**, 10166 (2006).

20. K.-H. Altmann, B. Pfeiffer, S. Arseniyadis, B. A. Pratt, K. C. Nicolaou, The chemistry and biology of epothilones--the wheel keeps turning. *ChemMedChem.* **2**, 396 (2007).

21. R. J. Lechleider *et al.*, Ixabepilone in combination with capecitabine and as monotherapy for treatment of advanced breast cancer refractory to previous chemotherapies. *Clin. Cancer Res.* **14**, 4378 (2008).

22. D. Zurwerra *et al.*, Total Synthesis of (-)-Zampanolide and Structure-Activity Relationship Studies on (-)-Dactylolide Derivatives. *Chem. Eur. J.* (2012).

23. N. Olieric *et al.*, Automated seamless DNA co-transformation cloning with direct expression vectors applying positive or negative insert selection. *BMC. Biotechnol.* **10**, 56 (2010).

24. J. M. Andreu, Large scale purification of brain tubulin with the modified Weisenberg procedure. *Methods Mol. Med.* **137**, 17 (2007).

25. W. Kabsch, XDS. *Acta Crystallogr. D. Biol. Crystallogr.* **66**, 125 (2010).

26. A. J. McCoy *et al.*, Phaser crystallographic software. *J Appl Crystallogr.* **40**, 658 (2007).

27. P. D. Adams *et al.*, PHENIX: a comprehensive Python-based system for macromolecular structure solution. *Acta Crystallogr. D. Biol. Crystallogr.* **66**, 213 (2010).

28. P. Emsley, K. Cowtan, Coot: model-building tools for molecular graphics. *Acta Crystallogr. D. Biol. Crystallogr.* **60**, 2126 (2004).

29. I. W. Davis, L. W. Murray, J. S. Richardson, D. C. Richardson, MOLPROBITY: structure validation and all-atom contact analysis for nucleic acids and their complexes. *Nucleic Acids Res.* **32**, W615 (2004).

30. P. A. Karplus, K. Diederichs, Linking crystallographic model and data quality. *Science* **336**, 1030 (2012).

31. A. E. Prota, M. M. Magiera, M. Kuijpers, K. Bargsten, D. Frey, M. Wieser, R. Jaussi, C. C. Hoogenraad, R. A. Kammerer, C. Janke, M. O. Steinmetz, Structural basis of tubulin tyrosination by tubulin tyrosine ligase. *J. Cell Biol.*, in press. DOI: 10.1083/jcb.201211017.